Interaction-induced gradients across a confined fermion lattice

G. George Batrouni[1] and Richard T. Scalettar[2]
[1]*Université Côte d'Azur, INPHYNI, Centre National de la Recherche Scientifique, 0600 Nice, France*
[2]*Department of Physics, University of California Davis, Davis, California 95616, USA*
(Received 16 July 2017; published 26 September 2017)

An imposed chemical potential gradient $A_\uparrow = d\mu_\uparrow/dx$ on a *single* fermionic species ("spin up") directly produces a gradient in the density $d\rho_\uparrow/dx$ across a lattice. We study here the *induced* density inhomogeneity $d\rho_\downarrow/dx$ in the second fermionic species ("spin down") which results from fermionic interactions U, even in the absence of a chemical potential gradient $A_\downarrow = 0$ on that species. The magnitude of $d\rho_\downarrow/dx$ acquired by the second species grows with U, while the magnitude of $d\rho_\uparrow/dx$ remains relatively constant, that is, set only by $A_\uparrow$. For a given $A_\uparrow$, we find an interaction strength U_* above which the two density gradients are equal in magnitude. We also evaluate the spin-spin correlations and show that, as expected, antiferromagnetism is most dominant at locations where the local density is half filled. The spin polarization induced by sufficiently large gradients, in combination with U, drives ferromagnetic behavior. In the case of repulsive interactions, $d\rho_\downarrow/dx = -d\rho_\uparrow/dx$. A simple particle-hole transformation determines the related effect in the case of attractive interactions.

DOI: 10.1103/PhysRevA.96.033632

I. INTRODUCTION

Over the past several years, there has been a great deal of progress in realizing antiferromagnetic (AF) correlations in trapped fermionic gases [1–5]. Therefore, understanding the effects of chemical potential gradients has become a central objective of quantum simulations of Hubbard Hamiltonians modeling bosonic or fermionic atoms on optical lattices. The most common situation studied is a confining potential which rises smoothly from the center of the system. An immediate consequence is the presence and coexistence of a sequence of phases, superfluid, and Mott insulator in the bosonic case [6–10] and band insulator, metallic, and antiferromagnetic insulator for fermions [11–14], as one moves radially outward from the trap center. With two fermionic species, the focus is almost exclusively on the situation in which the confining potential acts equally on "spin up" and "spin down," so that the densities of the species, although varying spatially, do so in lock step with each other.

In addition to the density variation across the lattice, and the accompanying local phases, the behavior of the thermodynamics is of considerable interest: The prospect of regions of the gas acting as local entropy reservoirs has implications for adiabatic cooling as the lattice is turned on, and the possibility of achieving longer-range antiferromagnetic correlations [13,15]

Although spin-dependent potentials are atypical in the condensed-matter context, they are possible to achieve in the case of optically trapped atoms where the fermionic species correspond to different hyperfine states. As an example, "spin-dependent" optical lattices have been discussed some time ago and their usefulness in thermometry and prospect for achieving exotic pairing states explored [16–19]. Similarly, the properties of disordered systems in which the *randomness* is spin dependent (and the interactions are attractive) have been explored within a Bogoliubov–de Gennes approach leading to unusual gapless superconducting phases and phase transitions [20,21]. In the condensed-matter context, such spin-dependent disorder is closely related to the problem of magnetic impurities in a superconductor [22].

The present paper is motivated by recent reports of measurements on trapped fermionic gases in the presence of species-dependent gradients [23]. One could envision generating a similar situation in a condensed-matter context through the application of an in-plane Zeeman-coupled magnetic-field gradient. The results here serve to quantify the induced density gradient $\rho_\downarrow(x)$ and double occupancy $D(x)$ for specific values of the interaction strength U, temperature T, and chemical potential gradient $A_\uparrow$ which would arise in such realizations. Of particular note are the following results.

(i) The induced density gradient in $\rho_\downarrow$ converges to that of $\rho_\uparrow$ when U is made sufficiently large $U > U_*$.

(ii) Through a suitable definition of the "characteristic density," defined below, data for different gradients A can be scaled together on a universal curve.

(iii) Both the direct and induced density gradients initially grow linearly with A, but while, at large enough A, the density difference across the lattice approaches unity, if $U < U_*$ the induced gradient reaches a plateau which does not reflect full suppression or enhancement of density at the lattice edges.

(iv) Nearest-neighbor spin correlations become ferromagnetic at the lattice edge for high gradients.

II. MODEL AND METHODOLOGY

We consider the Hubbard Hamiltonian,

$$H = -t\sum_{\langle ij\rangle\sigma}(c^\dagger_{i\sigma}c_{j\sigma} + c^\dagger_{j\sigma}c_{i\sigma}) + U\sum_i\left(n_{i\uparrow}-\frac{1}{2}\right)\left(n_{i\downarrow}-\frac{1}{2}\right) - \sum_{i\sigma}\mu_\sigma(i)\,n_{i\sigma}, \quad (1)$$

with the usual kinetic energy, parameterized by t, describing hopping between nearest-neighbor sites $\langle ij\rangle$ on a two-dimensional square lattice, and on-site repulsion U. We choose $t = 1$ to set the scale of the energy.

 ©2017 American Physical Society

The chemical μ is chosen to be spin dependent:

$$\mu_\downarrow(x) = 0,$$
$$\mu_\uparrow(x) = A\left(x - \frac{n-1}{2}\right). \quad (2)$$

Here $x = 0,1,2,\ldots,n-1$ labels the x coordinate of the site $i = (x,y)$. The form in Eq. (2) makes $\mu_\sigma = 0$ at the center of the lattice and the average chemical potentials across the whole lattice, $\langle\mu_\sigma\rangle = 0$. Therefore, the filling is close to $\rho_\sigma = 0.5$ (half filling). In most of our plots we have chosen $n \times n$ lattices with $n = 12$, and periodic boundary conditions along y and open ones along x.

It is simple to understand quantitatively the effect of the μ gradient using mean-field theory (MFT) where the interaction term is decoupled so that the down-spin fermions see $+U\langle n_{i\uparrow}\rangle$. Since $\langle n_{i\uparrow}\rangle$ decreases as x increases, due to $\mu_\uparrow$, down-spin fermions see a lower (more negative) chemical potential $\mu_{i\downarrow}^{\rm mft} = -U\langle n_{x\uparrow}\rangle$ at one edge of the lattice, $i_x = 0$, than at the other, $i_x = n-1$. This MFT-induced chemical potential gradient introduces an effective density gradient for the down-spin fermions as well.

While one could formalize such a MFT treatment, we instead present here the results of determinant quantum Monte Carlo (DQMC) simulations [24], which treat the effects of U exactly. In DQMC, the interaction term is decoupled by introducing a space and imaginary time-dependent Hubbard-Stratonovich (HS) field. The integration over this field, with Monte Carlo, fully restores the effect of U, to within the fully controlled errors introduced by the discretization of the inverse temperature $\beta = L\Delta\tau$. Here we choose $\Delta\tau$ small enough so that these "Trotter errors" [25–27] are of the order of a few percent. Most existing DQMC treatments of confined fermions [15] or inhomogeneous systems generally [28] utilize the local density approximation, in order to analyze systems of larger size. The spatial resolution of DQMC, however, allows the exact treatment of gradients beyond the LDA. We perform such a treatment here.

Because of the nonvanishing $\mu_\uparrow(x)$, the weight associated with individual HS field configurations can become negative leading to a "sign problem" [29,30]. However, since we keep the lattice roughly half filled by the choice of $\mu_\sigma(i)$ in Eq. (2), we find the sign problem to be quite mild. A similar mitigation of the sign problem is found in a bilayer system when one sheet is electron doped and the other is hole doped symmetrically [31].

In the absence of gradients, powerful finite-size scaling methods have been developed both in classical and quantum Monte Carlo to extract information about the thermodynamic limit from lattices of finite size. In the commonly studied case of confined lattices, the notions of "characteristic density" and "characteristic length" were developed [32–34] in order to study and compare systems with different sizes. The idea is to define appropriate length scales associated with the nonuniformity in the system and use them to define an effective characteristic density. In Eqs. (1) and (2), the parameter A/a has the units of energy/length (a is the lattice constant). Then a characteristic length can be defined in the x direction, $\xi \equiv at/A$, while in the y direction, which has no gradient, the characteristic length remains n. The characteristic up-spin density is then $\tilde{\rho}_\uparrow \equiv N_\uparrow/(n\xi) = \rho_\uparrow An/t$, where $\rho_\uparrow \equiv N_\uparrow/n^2$. Similar definitions apply for the down spins. We show below that systems with different sizes will display the same properties if they are at a common value of $\tilde{\rho}$, in analogy to what happens in traps [32–34].

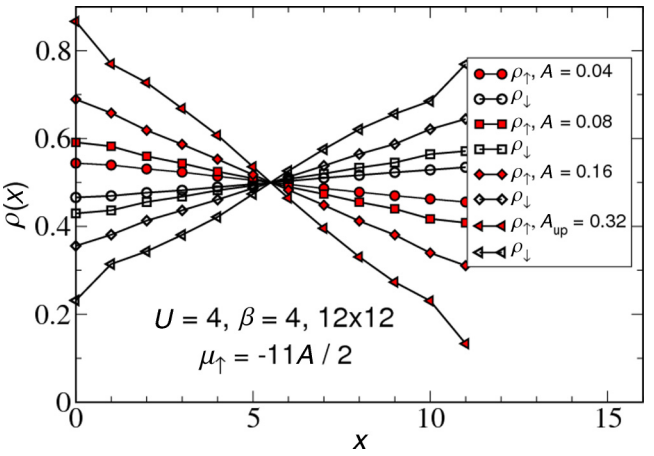

FIG. 1. Fermionic density gradients on a 12×12 lattice at $\beta = 4$ and $U = 4$. Only the up fermions experience a chemical potential gradient [see Eq. (1)] but the interactions force the down fermion density to respond in an anticorrelated way.

III. RESULTS: LOCAL DENSITY

We begin by showing, in Fig. 1, the density gradients which arise from different up-spin chemical potential gradients A. The interaction strength $U = 4$ and inverse temperature $\beta = 4$ are kept fixed. As suggested by the mean-field theory picture, the down-spin fermions acquire a gradient, even though the chemical potential they experience is spatially flat.

The data of Fig. 2 address the question of finite-size scaling by quantifying the density profiles for three system sizes such that the characteristic density remains constant. We chose $A = \delta\mu/(n-1)$ with $\delta\mu = 0.88$, the chemical potential difference between the edges of the system, kept constant leading to a

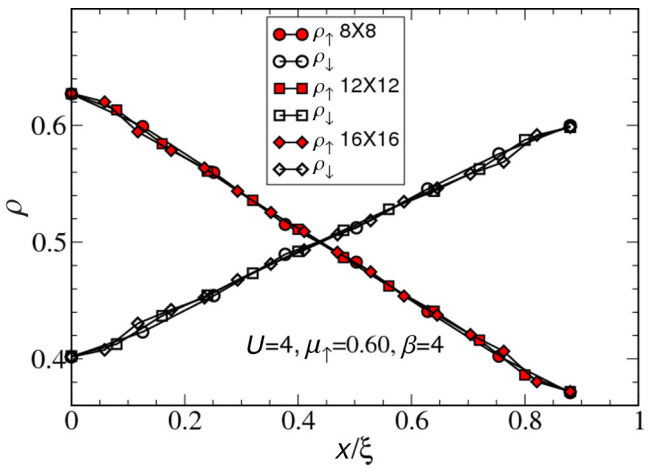

FIG. 2. Density profile collapse for $n = 8,12,16$ vs the characteristic coordinate, x/ξ. The simulations are at the same $\tilde{\rho}$ (see text).

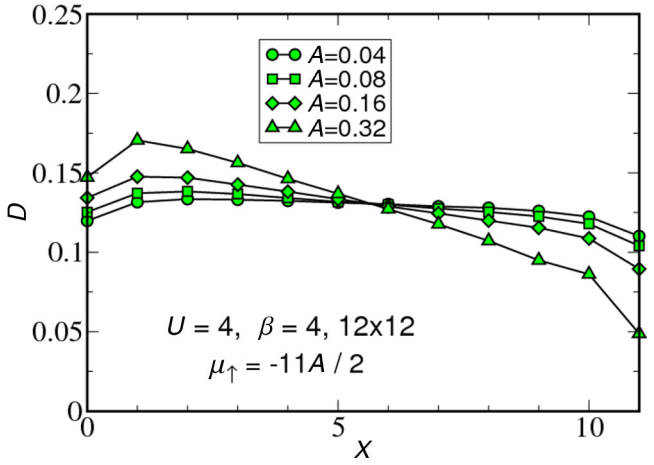

FIG. 3. Double occupancy D vs position. $U = 4$ and $\beta = 4$ are fixed. The up fermion chemical potential gradient, A, varies as indicated. D is fairly constant across the lattice for weak gradients, but is markedly asymmetric for stronger gradients, at this value of U.

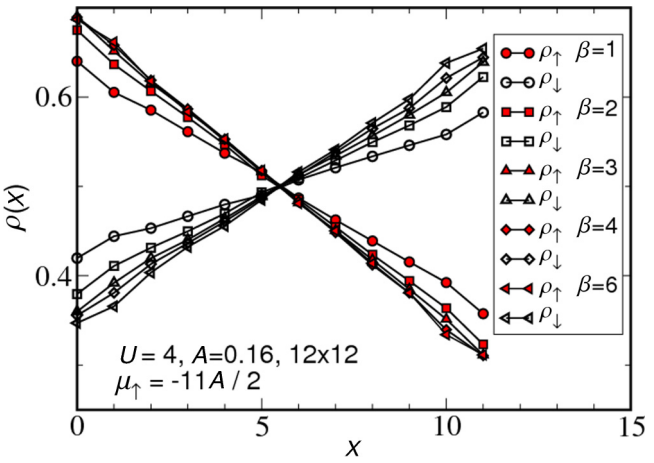

FIG. 5. Fermionic density gradients on a 12×12 lattice at $U = 4$ and $A = 0.16$ Only the up fermions experience a chemical potential gradient [see Eq. (1)]. For this strength of chemical potential gradient, the density has achieved its low T value at $\beta \sim 4$.

constant $\tilde{\rho}_\uparrow = \rho_\uparrow \delta\mu/t$. When the density profiles are plotted against the characteristic position, x/ξ, $\xi = at/A$, we obtain excellent collapse of the data.

The double occupancy profile across the lattice is shown in Fig. 3 for $U = 4$, $\beta = 4$, and different gradients A. This value of U is not sufficient to impose a down-spin density gradient as large as the up-spin gradient: The enhancement of $\rho_\downarrow$ for $x = n - 1$ is not developed fully enough to compensate for the direct reduction in $\rho_\uparrow$ by A, and hence D is lower than at $x = 0$.

Figure 4 shows the effect of varying U at fixed up-spin chemical potential gradient $A = 0.08$ and inverse temperature $\beta = 4$. The up-spin density gradient is largely independent of U whereas, as expected, the induced down-spin density gradient develops more and more fully as U grows. This

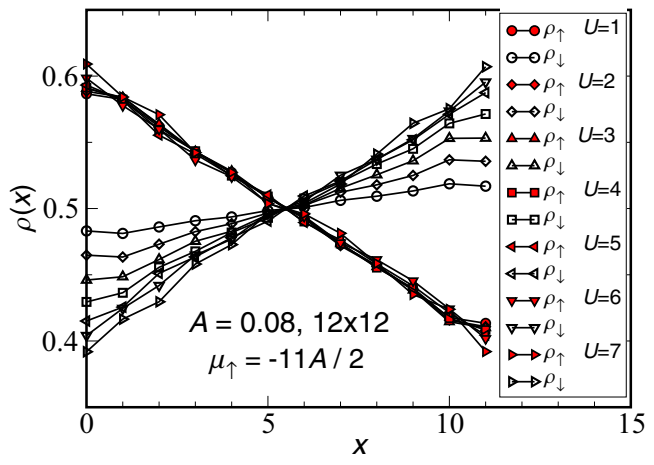

FIG. 4. Fermionic density gradients on a 12×12 lattice at $\beta = 4$ and $A = 0.08$. Only the up fermions experience a chemical potential gradient [see Eq. (1)]. As is reasonable, when U is small, the down gradient is less noticeable. (Obviously it would vanish at $U = 0$.) What is not completely expected is the almost complete insensitivity of $\rho_\uparrow(x)$ to U.

observation is not completely captured within MFT. One might expect that, as a nontrivial down-spin profile develops, it would act to reinforce the up-spin density gradient by further lowering the energy cost for putting up spin fermions at $x = 0$ and raising it at $x = n - 1$. This is, however, not a noticeable effect, at least for the parameters shown in Fig. 4 (see also Fig. 7.)

Figure 5 quantifies the typical temperature scales needed to establish the gradients for the A and U values in Figs. 1–4. By the time $\beta \sim 4$ ($T = t/4$) the density gradients at $U = 4$ and $A = 0.16$ have reached their asymptotic values.

Collectively, Figs. 1, 4, and 5 provide precise quantitative benchmarks for the magnitude of interaction-induced gradients as (i) the direct gradient, (ii) the interaction strength, and (iii) the temperature are varied, respectively.

Inspection of the density gradients in the preceding figures already suggests that they grow roughly linearly in A. This is verified more explicitly in Fig. 6 by the data for the overall edge-to-edge density differences:

$$d\rho_\sigma = |\rho_\sigma(x = 0) - \rho_\sigma(x = n - 1)|. \tag{3}$$

A linear growth (albeit with a different slope for the two spin species) occurs over a wide range of A. This is followed, at large A, by a plateau of the up-spin density at full "polarization," where $\rho_\uparrow(x = 0) \to 1$ and $\rho_\uparrow(x = n - 1) \to 0$, so that $d\rho_\uparrow \to 1$. The down-spin polarization saturates at a reduced value. Within the MFT picture introduced earlier, the induced down-spin chemical potential gradient is bounded by U. Since $U = 4$ in Fig. 6 is only half the kinetic-energy bandwidth, the induced gradient is insufficient fully to localize the down-spin fermions at the $x = n - 1$ edge. This accounts for the incomplete saturation of $d\rho_\downarrow$.

It is interesting to explore the variation of $d\rho_\sigma$ with U, as done in Fig. 7. One sees that the up-spin density gradient does in fact grow with U, as the MFT picture discussed in the context of Fig. 4 might suggest, but does so only weakly. The induced down-spin gradient evolves much more rapidly, ultimately achieving, for $A = 0.08$, parity at $U = U_* \sim 6$, where the up and down density gradients fully match up. The

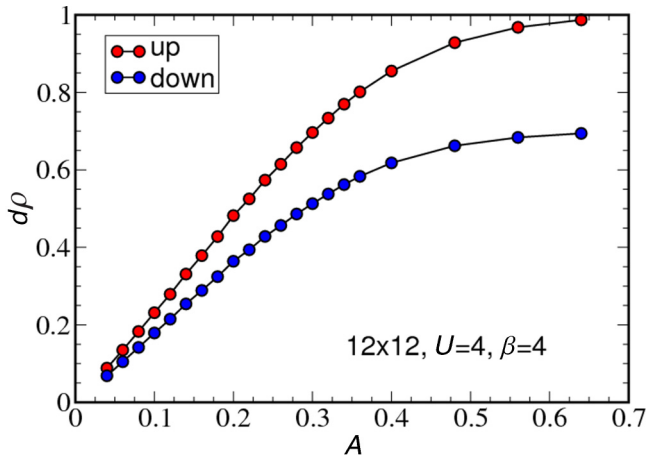

FIG. 6. Absolute value of the difference $d\rho$ between the densities at the two edges of box. At fixed U, as A increases, the down-spin gradient is less able to follow the up-spin gradient, and ultimately saturates at less than the full value $d\rho_\uparrow = 1$ corresponding to densities $\rho_\uparrow = 0,1$ at the lattice edges. Note that most of the preceding data were for the regime of relatively small A, where the slopes are linear.

inset shows the dependence of the value of U at which the up and down density gradients become equal, as a function of the size of the gradient. The dependence is seen to be rather weak. We believe this is so because U_* is set not only by A but also by the quantum fluctuations (that is, the fermionic hopping parameter t) which act to equalize the density across the lattice.

IV. RESULTS: LOCAL SPIN CORRELATIONS

In this section, the behavior of the local AF correlations across the sample box is described. Naively, as is the case for fermions confined in a quadratic potential, one expects the antiferromagnetic spin response to be maximal where the

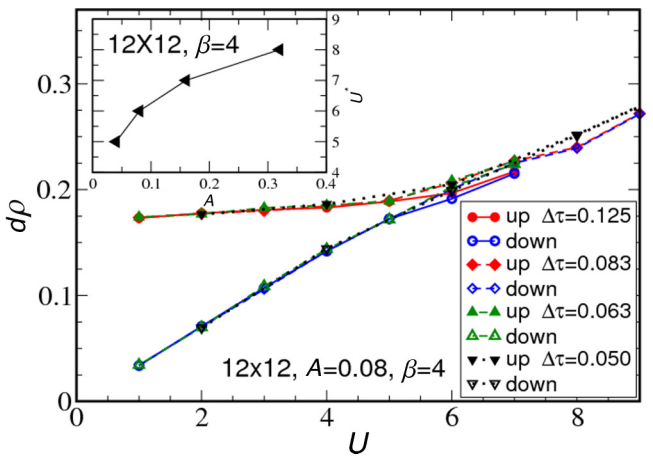

FIG. 7. Absolute value of difference $d\rho$ between densities at the two edges of the box. The induced difference $d\rho_\downarrow$ achieves parity with the direct difference $d\rho_\uparrow$ at $U = U_* \sim 6$. Data for different values of the inverse temperature discretization $\Delta\tau$ indicate that Trotter errors are, at largest, comparable to fluctuations associated with the statistical sampling. The inset shows the dependence of U_* on A.

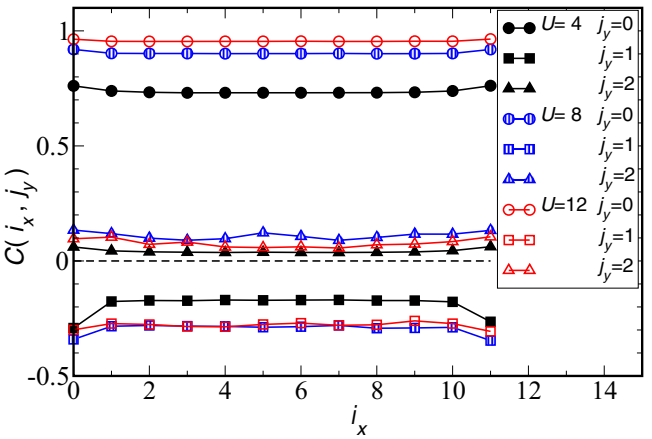

FIG. 8. Spin-spin correlation function $c(i_x, j_y)$ at three values of the on-site interaction $U = 4,8,12$. Here $\beta = 4$, the gradient $A_\uparrow = 0$, and the lattice is 12×12. Magnetism is enhanced at the edges of the lattice $i_x = 0$ and $n - 1$ as a consequence of the OBC.

local density is close to half -filling. Here, with the choice of gradient, Eq. (2), this corresponds to the equipotential line, $\mu = 0$, in the center of the box. This expectation is confirmed, and, in addition, we discuss edge effects due to open boundary conditions in the gradient ($\hat{x}$) direction.

We define the correlation function between a spin on site (i_x, i_y) and one that is separated by a distance j_y in the $\hat{y}$ direction, transverse to the gradient (i.e., at the same chemical potential):

$$c^{\alpha\alpha}(i_x, j_y) = \left\langle S^\alpha_{i_x, i_y + j_y} S^\alpha_{i_x, i_y} \right\rangle,$$
$$S^\alpha_{i_x, i_y} = \left(c^\dagger_{i_x i_y \uparrow} \quad c^\dagger_{i_x i_y \downarrow}\right) \sigma^\alpha \begin{pmatrix} c_{i_x i_y \uparrow} \\ c_{i_x i_y \downarrow} \end{pmatrix}, \tag{4}$$

where σ^α is a Pauli spin matrix. Because of periodic boundary conditions in the $\hat{y}$ direction, this quantity is independent of i_y, as suggested by the notation, which also serves to emphasize the distinction between the two lattice directions, only one of which is subject to the chemical potential gradient. The local moment is given by $\langle m^2(i_x) \rangle = c(i_x, j_y = 0)$, and the nearest-neighbor spin correlator is given by $c(i_x, j_y = 1)$. In the data which follow, we average $c^{\alpha\alpha}$ over the three rotationally equivalent spin directions $\alpha = x, y, z$.

Figure 8 exhibits the spin correlators for $j_y = 0,1,2$ as functions of position in the $\hat{x}$ direction in the *absence* of a gradient. A characteristic AF pattern is observed, with a large positive local moment ($j_y = 0$), negative nearest-neighbor ($j_y = 1$) correlations, and positive next-nearest-neighbor ($j_y = 2$) correlations. The absolute value of $c(i_x, j_y)$ decreases with j_y since the temperature $T = t/4$ is not much below $J \sim t^2/U$. Nevertheless, one can observe some of the crucial characteristic features of AF correlations in the Hubbard Hamiltonian: a local moment which increases monotonically with U, and a maximum in magnetism at intermediate $U \sim 8$ reflecting the initial growth of magnetism at weak U followed by a decline at finite T at strong coupling as the exchange constant J falls.

It is useful to understand this behavior of $c(i_x, i_y)$ at $A_\uparrow = 0$ because, even in the absence of a gradient, translational

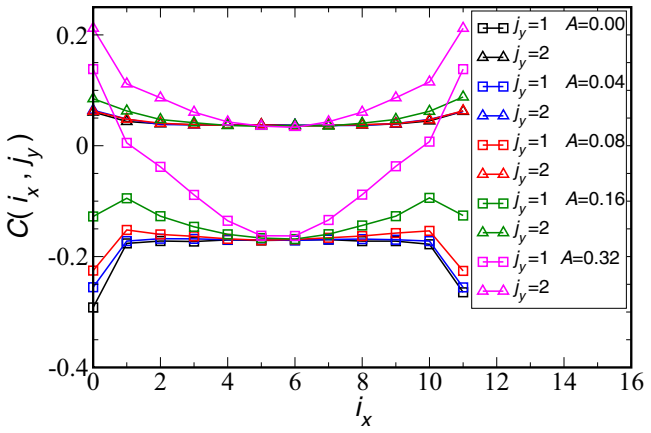

FIG. 9. Spin-spin correlation function $c(i_x, j_y)$ at fixed $U = 4$ and different values of the gradient $A = 0.00, 0.04, 0.08, 0.16$, and 0.32. Here $\beta = 4$, and the lattice is 12×12.

invariance is still broken by the open boundary conditions in the $\hat{x}$ direction. This manifests itself as an *enhancement* of magnetism at the boundaries ($i_x = 0$ and $i_x = n - 1$) which is especially evident in the nearest-neighbor correlation at $U = 4$. Such enhancement is known to occur in a variety of materials, and can be ascribed either to the reduced coordination at the surface and the associated lowering of quantum fluctuations (as is the case here), or to the presence of modified exchange constants due to surface relaxation or reconstruction [35].

Having exhibited this surface enhancement, Fig. 9 shows the effect of different gradients on the spin correlations at $U = 4$. Consider first the nearest-neighbor correlation $c(i_x, j_y = 1)$, which becomes less negative as $A_\uparrow$ increases: the gradient, in combination with the on-site repulsion, polarizes the fermionic density and suppressed antiferromagnetism. Indeed, for sufficiently large values of the gradient, the nearest-neighbor spin correlator becomes *positive* (ferromagnetic) at the edges of the trap, while remaining negative, with a value which is independent of $A_\uparrow$, at the lattice center $i_x = (n - 1)/2$. [The constancy of $c(i_x = (n - 1)/2, i_y)$ can be viewed as an indication that the local-density approximation is valid: the magnetism depends only on the density, which is $\rho_\sigma = 1/2$, and not strongly on the gradient.] The next-nearest-neighbor correlator, $c(i_x, j_y = 2)$, which is already ferromagnetic in the absence of a gradient, becomes larger in magnitude with increasing $A_\uparrow$.

The position and spin-dependent chemical potentials $\mu_\sigma(x)$ in Eq. (2) can equivalently be written as a spin-*independent* (but still spatially varying) chemical potential, combined with a position dependent Zeeman field:

$$\mu'(x) = B(x) = -\frac{A}{2}\left(x - \frac{n-1}{2}\right). \tag{5}$$

Equation (5) is easily seen to be equivalent to Eq. (2) by noting that $\mu_\uparrow(x) = B(x) + \mu'(x)$ and $\mu_\downarrow(x) = -B(x) + \mu'(x)$. This provides an alternate understanding of the spin polarization, and hence ferromagnetic correlations at the lattice edges.

V. CONCLUSIONS

In this paper, we explored the effect of a spin-dependent chemical potential gradient on a confined electron gas. *Homogeneous* spin-dependent potentials (Zeeman fields) have, of course, been extensively studied within the context of pairing in spin-imbalanced systems (Fulde-Ferrell-Larkin-Ovchinnikov superconductivity [36–38]). Similarly, as noted in the introduction, spatially disordered spin-dependent chemical potentials can produce novel superconductivity in the presence of attractive interactions. They also have been shown to have interesting consequences for metal-insulator transitions (MITs), sharing the qualitative behavior of bond randomness, but behaving quite distinctly from spin-independent disorder [39]. The combination of different types of spin-dependent and -independent fields likewise can drive systems across the MIT [40].

The anticorrelated gradient of charge of two spin species caused by an on-site repulsion U is similar in physical origin, and qualitative consequences, to the transfer of charge between distinct orbitals in condensed-matter systems. In a three-band model of cuprate superconductors, for example, a difference in oxygen p and copper d single-particle energy $\Delta_{pd} = \epsilon_p - \epsilon_d$ leads to an "orbital occupation gradient." An interesting interplay then occurs between Δ_{pd} and the intersite Coulomb interaction V_{pd}. For example, as the total density of the system increases, there can be a counterintuitive decrease in oxygen p occupation [41]. Thus, although the realization of distinct potentials for different spin species is considerably more challenging in the condensed-matter context than in trapped atomic systems, some of the underlying physics might be quite analogous in considering the "orbital label" rather than the spin one.

Evaluation of local spin correlations, and their dependence on local density, has been a crucial objective of QMC studies of trapped fermionic gases, since this leads to an identification of the spatial extent of the region in which long-range antiferromagnetism might be observed experimentally [1–4]. We have examined here the case of a linear gradient, complementing previous work in quadratic traps. Most studies of a quadratic trap consider situations in which the density falls to zero at the box edge, and hence spin correlations are small. A key observation in this paper is that, in the case of moderate gradients in which the density remains nonzero at the box edge, there can be an enhancement of AF correlations due to the reduction of quantum fluctuations at the "surface" of the sample caused by the open boundary conditions. These correlations ultimately become ferromagnetic at large gradients.

A particle-hole transformation $c_{i\uparrow} \to (-1)^i c^\dagger_{i\uparrow}$ maps the repulsive Hubbard Hamiltonian onto the attractive Hubbard Hamiltonian [42,43]. Since $n_{i\uparrow} \to 1 - n_{i\uparrow}$, the chemical potential gradient reverses sign, as does the associated up-spin density gradient. Since there is no transformation of the down-spin operators, the induced down-spin gradient is unchanged in sign, and we see that, as expected, in an attractive model, $d\rho_\downarrow/dx$ and $d\rho_\uparrow/dx$ have the same sign.

ACKNOWLEDGMENTS

This paper was supported by the U.S. Department of Energy, Office of Science, Office of Basic Energy Sciences under Grant No. DE-SC0014671 (R.T.S.).

[1] R. A. Hart, P. M. Duarte, T. Yang, X. Liu, T. Paiva, E. Khatami, R. T. Scalettar, N. Trivedi, D. A. Huse, and R. G. Hulet, Observation of antiferromagnetic correlations in the Hubbard model with ultracold atoms, Nature (London) **519**, 211 (2015).

[2] P. M. Duarte, R. A. Hart, T.-L. Yang, X. Liu, T. Paiva, E. Khatami, R. T. Scalettar, N. Trivedi, and R. G. Hulet, Compressibility of a Fermionic Mott Insulator of Ultracold Atoms, Phys. Rev. Lett. **114**, 070403 (2015).

[3] L. W. Cheuk, M. A. Nichols, K. R. Lawrence, M. Okan, H. Zhang, E. Khatami, N. Trivedi, T. Paiva, M. Rigol, and M. W. Zwierlein, Observation of spatial charge and spin correlations in the 2D Fermi-Hubbard model, Science **353**, 1260 (2016).

[4] A. Mazurenko, C. S. Chiu, G. Ji, M. F. Parsons, M. Kanász-Nagy, R. Schmidt, F. Grusdt, E. Demler, D. Greif, and M. Greiner, Experimental realization of a long-range antiferromagnet in the Hubbard model with ultracold atoms, Nature (London) **545**, 462 (2017).

[5] P. T. Brown, D. Mitra, E. Guardado-Sanchez, P. Schauss, S. S. Kondov, E. Khatami, T. Paiva, N. Trivedi, D. A. Huse, and W. S. Bakr, Observation of canted antiferromagnetism with ultracold fermions in an optical lattice, arXiv:1612.07746.

[6] G. G. Batrouni, V. Rousseau, R. T. Scalettar, M. Rigol, A. Muramatsu, P. J. H. Denteneer, and M. Troyer, Mott Domains of Bosons Confined on Optical Lattices, Phys. Rev. Lett. **89**, 117203 (2002).

[7] B. DeMarco, C. Lannert, S. Vishveshwara, and T.-C. Wei, Structure and stability of Mott-insulator shells of bosons trapped in an optical lattice, Phys. Rev. A **71**, 063601 (2005).

[8] G. K. Campbell, J. Mun, M. Boyd, P. Medley, A. E. Leanhardt, L. G. Marcassa, D. E. Pritchard, and W. Ketterle, Imaging the Mott insulator shells by using atomic clock shifts, Science **313**, 649 (2006).

[9] R. A. Barankov, C. Lannert, and S. Vishveshwara, Coexistence of superfluid and Mott phases of lattice bosons, Phys. Rev. A **75**, 063622 (2007).

[10] K. Sun, C. Lannert, and S. Vishveshwara, Probing condensate order in deep optical lattices, Phys. Rev. A **79**, 043422 (2009).

[11] R. Jördens, N. Strohmaier, K. Günter, H. Moritz, and T. Esslinger, A Mott insulator of fermionic atoms in an optical lattice, Nature (London) **455**, 204 (2008).

[12] C. J. M. Mathy, D. A. Huse, and R. G. Hulet, Enlarging and cooling the Néel state in an optical lattice, Phys. Rev. A **86**, 023606 (2012).

[13] S. Fuchs, E. Gull, L. Pollet, E. Burovski, E. Kozik, T. Pruschke, and M. Troyer, Thermodynamics of the 3D Hubbard Model on Approaching the Néel Transition, Phys. Rev. Lett. **106**, 030401 (2011).

[14] U. Schneider, L. Hackermüller, S. Will, Th. Best, I. Bloch, T. A. Costi, R. W. Helmes, D. Rasch, and A. Rosch, Metallic and insulating phases of repulsively interacting fermions in a 3D optical lattice, Science **322**, 1520 (2008).

[15] T. Paiva, Y. L. Loh, N. Trivedi, M. Randeria, and R. T. Scalettar, Fermions in 3D Optical Lattices: Cooling Protocol to Obtain Antiferromagnetism, Phys. Rev. Lett. **107**, 086401 (2011).

[16] D. McKay and B. DeMarco, Thermometry with spin-dependent lattices, New J. Phys. **12**, 055013 (2010).

[17] O. Mandel, M. Greiner, A. Widera, T. Rom, T. W. Hänsch, and I. Bloch, Coherent Transport of Neutral Atoms in Spin-Dependent Optical Lattice Potentials, Phys. Rev. Lett. **91**, 010407 (2003).

[18] A. E. Feiguin and M. P. A. Fisher, Exotic Paired States with Anisotropic Spin-Dependent Fermi Surfaces, Phys. Rev. Lett. **103**, 025303 (2009).

[19] W. Vincent Liu, F. Wilczek, and P. Zoller, Spin-dependent Hubbard model and a quantum phase transition in cold atoms, Phys. Rev. A **70**, 033603 (2004).

[20] R. Nanguneri, M. Jiang, T. Cary, G. G. Batrouni, and R. T. Scalettar, Interplay of superconductivity and spin-dependent disorder, Phys. Rev. B **85**, 134506 (2012).

[21] M. Jiang, R. Nanguneri, N. Trivedi, G. G. Batrouni, and R. T. Scalettar, Novel gapless superfluid phase with spin-dependent disorder, New J. Phys. **15**, 023023 (2013).

[22] A. A. Abrikosov and L. P. Gorkov, Contribution to the theory of superconducting alloys with paramagnetic impurities, Sov. Phys. JETP **12**, 1243 (1961).

[23] M. Nichols, L. Cheuk, K. Lawrence, M. Okan, H. Zhang, E. Khatami, N. Trivedi, T. Paiva, M. Rigol, and M. Zwierlein, Site-Resolved Observation of Charge and Spin Correlations in the 2D Fermi-Hubbard Model, Session B9.00006, APS DAMOP 2017.

[24] R. Blankenbecler, D. J. Scalapino, and R. L. Sugar, Monte Carlo calculations of coupled boson-fermion systems. I, Phys. Rev. D **24**, 2278 (1981).

[25] H. F. Trotter, On the product of semi-groups of operators, Proc. Amer. Math. Soc. **10**, 545 (1959).

[26] M. Suzuki, Relationship between d-dimensional quantal spin systems and $(d+1)$-dimensional Ising systems: Equivalence, critical exponents and systematic approximants of the partition function and spin correlations, Prog. Theor. Phys. **56**, 1454 (1976).

[27] R. M. Fye, New results on Trotter-like approximations, Phys. Rev. B **33**, 6271 (1986).

[28] T. Paiva, E. Khatami, S. Yang, V. Rousseau, M. Jarrell, J. Moreno, R. G. Hulet, and R. T. Scalettar, Cooling Atomic Gases with Disorder, Phys. Rev. Lett. **115**, 240402 (2015).

[29] E. Y. Loh, J. E. Gubernatis, R. T. Scalettar, S. R. White, D. J. Scalapino, and R. L. Sugar, Sign problem in the numerical simulation of many-electron systems, Phys. Rev. B **41**, 9301 (1990).

[30] M. Troyer and U.-J. Wiese, Computational Complexity and Fundamental Limitations to Fermionic Quantum Monte Carlo Simulations, Phys. Rev. Lett. **94**, 170201 (2005).

[31] K. Bouadim, G. G. Batrouni, F. Hébert, and R. T. Scalettar, Magnetic and transport properties of a coupled Hubbard bilayer with electron and hole doping, Phys. Rev. B **77**, 144527 (2008).

[32] M. Rigol, A. Muramatsu, G. G. Batrouni, and R. T. Scalettar, Local Quantum Criticality in Confined Fermions on Optical Lattices, Phys. Rev. Lett. **91**, 130403 (2003).

[33] G. G. Batrouni, H. R. Krishnamurthy, K. W. Mahmud, V. G. Rousseau, and R. T. Scalettar, Canonical trajectories and critical coupling of the Bose-Hubbard Hamiltonian in a harmonic trap, Phys. Rev. A **78**, 023627 (2008).

[34] M. Rigol, G. G. Batrouni, V. G. Rousseau, and R. T. Scalettar, State diagrams for harmonically trapped bosons in optical lattices, Phys. Rev. A **79**, 053605 (2009).

[35] For a review, see F. Zhang, S. Thevuthasan, R. T. Scalettar, R. R. P. Singh, and C. S. Fadley, Monte Carlo study of magnetic order at ferromagnetic and antiferromagnetic surfaces: Implications for spin-polarized photoelectron diffraction, Phys. Rev. B **51**, 12468 (1995), and references cited therein.

[36] P. Fulde and A. Ferrell, Superconductivity in a strong spin-exchange field, Phys. Rev. **135**, A550 (1964).

[37] A. Larkin and Y. N. Ovchinnikov, Nonuniform state of superconductors, Zh. Eksp. Teor. Fiz. **47**, 1136 (1964) [Sov. Phys. JETP **20**, 762 (1965)].

[38] For a review of numerical work on FFLO physics with an emphasis on trapped atomic gases, see M. J. Wolak, B. Grémaud, R. T. Scalettar, and G. G. Batrouni, Pairing in a two-dimensional Fermi gas with population imbalance, Phys. Rev. A **86**, 023630 (2012).

[39] P. J. H. Denteneer, R. T. Scalettar, and N. Trivedi, Particle-Hole Symmetry and the Effect of Disorder on the Mott-Hubbard Insulator, Phys. Rev. Lett. **87**, 146401 (2001).

[40] P. J. H. Denteneer and R. T. Scalettar, Interacting Electrons in a Two-Dimensional Disordered Environment: Effect of a Zeeman Magnetic Field, Phys. Rev. Lett. **90**, 246401 (2003).

[41] R. T. Scalettar, S. R. White, D. J. Scalapino, and R. L. Sugar, Antiferromagnetic, charge-transfer, and pairing correlations in the three-band Hubbard model, Phys. Rev. B **44**, 770 (1991).

[42] R. T. Scalettar, E. Y. Loh, Jr., J. E. Gubernatis, A. Moreo, S. R. White, D. J. Scalapino, R. L. Sugar, and E. Dagotto, Phase Diagram of the Two-Dimensional Negative-U Hubbard Model, Phys. Rev. Lett. **62**, 1407 (1989).

[43] A. Moreo and D. J. Scalapino, Cold Attractive Spin Polarized Fermi Lattice Gases and the Doped Positive U Hubbard Model, Phys. Rev. Lett. **98**, 216402 (2007).